Hill Climbing MPPT Control of Large Wind Turbines

Özhan Atmaca
Elkon Marine and Electric Technologies R&D Center
Sakarya University of Applied Sciences
Sakarya, Turkey
oat@elkon-tr.com

Murat Karabacak
Department of Electrical and Electronics Engineering
Sakarya University of Applied Sciences
Sakarya, Turkey
muratkarabacak@sakarya.edu.tr

***Abstract*—This paper proposes a new Hill Climbing (HC) Maximum Power Point Tracking (MPPT) control for large wind turbines, where the wind rotor inertia is not possible to neglect in the MPPT control. In addition to the proposed MPPT control, an analytic design methodology for speed and current loops for the control of back to back converter is provided. Experimental study has been conducted based on a wind turbine emulator with an Induction Motor (IM) and Permanent Synchronous Generator (PMSM) mechanically coupled to the IM. Experimental results show that the proposed MPPT control captures more power from the wind than the conventional one by 8.22 %, for the same wind profile.**

Keywords—maximum power tracking, wind turbine, hill climbing, high inertia

I. INTRODUCTION

By means of MPPT control methods, the power can be captured from the wind at the maximum rate. Two essential points in MPPT control are correctly detecting and tracking of the Maximum Power Point (MPP). Generator Signal Feedback (GSF), Tip Speed Ratio (TSR), Optimal Torque Control (OTC), Power Signal Feedback (PSF), Wind Turbine Power Curves (WTPC), and Hill Climbing (HC) methods are employed in general [1,2]. GSF and OTC based MPPT methods needs a priori of the generator, it is the torque constant especially depending on the magnetic saturation. In GSF control method, MPP depends on the wind rotor inertia, which may lead to errors in MPPT control [3]. These drawbacks are referred by other researchers in [3,4,5]. TSR needs anemometers to measure wind speeds [6,7]. A single anemometer cannot measure the true average wind speed, so MPP is not possible to calculate exactly. TSR requires the exact model knowledge about the turbine, as well. It is also well-known that WTPC needs for the real test data. Traditional HC needs no priori; however, it cannot track MPP under sudden wind speed changes since neglecting the effect of wind rotor inertia [8]-[12]. The wrong directionality is another possible problem for especially large-inertia turbines [13,14].

This paper proposes a new HC method relaxes the problems of the traditional one. Decoupling based PI controller designs are provided in the paper in section II. The proposed HC is given in section III, and then experimental study is presented in section IV. The last section is left for the conclusions. In results, traditional and proposed HC methods are compared to each other in terms of the captured power from the same wind profile.

Wind turbine research studies generally require a turbine emulator, it is a mechanical-exciting actuator. To emulate a wind turbine, it is necessary to control IM as a mechanical actuator in this study torque depending on the turbine model as:

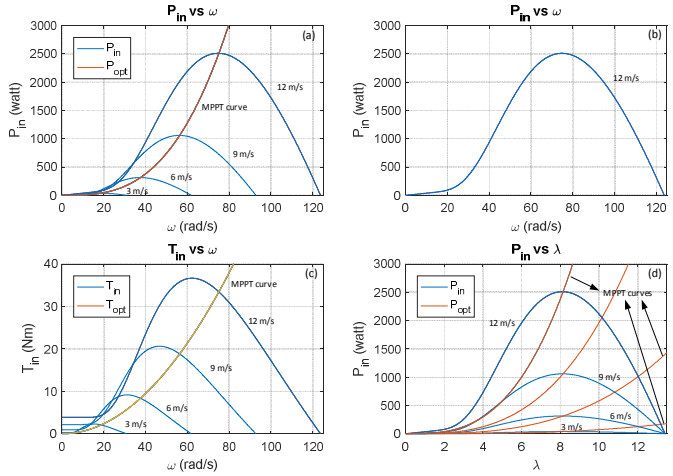

Fig. 1. Wind turbine response for wind speeds of 3, 6, 9 and 12 m/s: (a), (b) P_{in} *vs* ω*;* (c) T_{in} vs ω*;* and (d) P_{in} *vs* λ *()*

$$T_{in} = P_{in}/\omega_r = C_p P_w/\omega_r = 0.5\rho\pi R^5 C_p\left(\omega_r^2/\lambda^3\right) - J_r\dot{\omega}_r \quad (1)$$

$$P_{in} = C_p P_w = 0.5 C_p \rho A V^3 - J_r\omega_r\dot{\omega}_r \quad (2)$$

$$C_p(\lambda,\beta) = c_1\left(c_2/\lambda_i - c_3\beta - c_4\right)e^{\left(-c_5/\lambda_i\right)} + c_6\lambda \quad (3)$$

$$1/\lambda_i = 1/\left(\lambda + 0.08\beta\right) - 0.035/\left(\beta^3 + 1\right) \quad (4)$$

where A is the swept area of the propeller. β is the pitch angle and its value is zero in this study. σ is the air density, V is the wind speed, λ is the tip speed ratio, ω_r is the speed of wind rotor, C_p is the turbine power coefficient, P_{in} is the extracted power from the wind, T_{in} is the torque of wind rotor, J_r is the inertia of wind rotor, P_w is the available power in the wind. Coefficients $(C_1, C_2, C_3, C_4, C_5, C_6)$ appeared in Eq. (3) are given in Table 1. Eqs. (1)-(4) define the turbine model. Fig. 1 shows turbine responses and MPPT curves for different wind speeds. In Fig. 3, schematic of the turbine model is given.

Remark 1. J_{IM} and J_{PMSM} are inertias of IM and Permanent Magnet Synchronous Generator (PMSG) respectively. Total inertia at generator side is $J_{mT} = J_{IM} + J_{PMSM} + J_r N^2$. N is the virtual gear ratio, $3/4$. The wind rotor inertia, J_r, can also be emulated for any value as it is needed [15].

II. CONTROL OF BACK TO BACK CONVERTER

A. Rotor Field Oriented Control of Turbine Generator

Vector control, in short, of PMSG is implemented in such a way that q axis current delivers the desired torque while q axis

978-1-7281-7116-6/20/$31.00 ©2020 IEEE

current adjusts magnitude of the rotor flux density. Dynamical equations of the vector control are as follows [16,17]:

$$V_{dg} = \underbrace{R_s i_{dg} + L_{dg}\dot{i}_{dg}}_{V_{dg,PI}} + \underbrace{\left(-\omega_g L_{qg} i_{qg}\right)}_{V_{dg,coupling}} \quad (5)$$

$$V_{qg} = \underbrace{R_s i_{qg} + L_{qg}\dot{i}_{qg}}_{V_{qg,PI}} + \underbrace{\left(\omega_g L_{dg} i_{dg} + \omega_g \lambda_m\right)}_{V_{qg,coupling}} \quad (6)$$

$$J_{mT}\dot{\omega} = T_g - T_{in} \quad (7)$$

$$T_g = 1.5P\lambda_m i_{qg},\ k_t = 1.5P\lambda_m \quad (8)$$

where i_{dg} and i_{qg} are d and q axis currents, V_{dg} and V_{qg} are d and q axis voltages, R_s is the stator phase resistance, L_{dg} and L_{qg} are d and q axis inductances respectively, ω_g is the electrical speed, ω is the generator shaft speed, P is the pole-pairs, λ_m is the magnet flux, T_g is the generator torque, k_t is the torque constant. This PMSG is a surface magnet machine, thus the d axis desired current, i_{dgref}, is set to zero for satisfying maximum torque per ampere condition. $V_{dg,PI}$ and $V_{qg,PI}$ are the terms regulated by PI controllers, while $V_{dg,coupling}$ and $V_{qg,coupling}$ are compensated by the decoupling control. Eq. (8) is obtained setting $i_{dg} = 0$. All parameters of PMSG are given in Table 1. The decoupling control scheme is provided in Fig. 2, as well. PI gains should be chosen according to the desired settling time, 0.011 s, as;

$$K_{pdg} = k_{sett}\left(L_{dg} + L_d\right) \qquad K_{idg} = k_{sett}\left(R_s + R_d\right) \quad (9)$$

$$K_{pqg} = k_{sett}\left(L_{qg} + L_d\right) \qquad K_{iqg} = k_{sett}\left(R_s + R_d\right) \quad (10)$$

where L_d and R_d are inductance and resistance of inverter output filter. As shown in Fig. 2, ω_{opt} is the reference speed resulting from MPPT algorithm $k_{inv} = f_{cpeak}/\left(V_{dc}/\sqrt{3}\right)$, $f_{cpeak} = 3750$ (it is the peak value of PWM carrier wave) is PWM gain about 16.23 for 400 V DC bus voltage. PI gains are chosen so $K_{pdg} = \left(L_{qg} + L_d\right) = 0.004$, $K_{idg} = (R_s + R_d) = 0.5$, $K_{pqg} = \left(L_{dg} + L_d\right) = 0.0055$ and $K_{iqg} = (R_s + R_d) = 0.5$ that the closed loop transfer function of inner current loops is $TF_{cl} = 450/(s + 450)$ for $k_{sett} = 450$. In this case, settling time equals 0.011 s, which equals PMSM + filter electrical time constant. For $K_{pwg} = (J_{IM} + J_{PMSM}) = 0.0326$ and $K_{iwg} = B = 0.001$, and $k_{sett} = 100/3$, closed loop transfer function is obtained as:

Remark 2. $K_{pwg} = 0.0326$ is only valid for step response verification, In the generator control for MPPT control of wind turbine, $K_{pwg} = J_{mT} = 0.0326 + 6 \cdot 9/16 = 3.4076$ will be taken. Settling time of Eq. (11) equals about 0.15 s without an overshoot.

$$TF_{cl} = \frac{1.5e4s^2 + 6.75e6s}{s^4 + 900s^3 + 2.175e5s^2 + 6.75e6s} \quad (11)$$

In Fig. 3, all the closed loop control scheme is given along with the turbine emulator. But the emulator is kept out of scope in this study, to keep up with the page limit restriction of IEEE.

This study is supported by TUBITAK with the project of 114E159

B. Voltage Oriented Control of Grid Side Converter

Various kinds of control methods for the Grid Side Converter (GSC) have been proposed so far in the literature. Among all of them, voltage-oriented control is one of the most essential ones [18]-[20], given as:

$$V_{cd} = \underbrace{R_d i_{ds} + L_d\dot{i}_{ds}}_{V_{ds,PI}} + \underbrace{\left(-\omega_s L_q i_{qs} + V_{ds}\right)}_{V_{ds,coupling}} \quad (12)$$

$$V_{cq} = \underbrace{R_d i_{qs} + L_q\dot{i}_{qs}}_{V_{qs,PI}} + \underbrace{\left(\omega_s L_d i_{ds} + V_{qs}\right)}_{V_{qs,coupling}} \quad (13)$$

$$\dot{V}_{dc}^2 = \left(3V_{ds}/2C_{dc}\right)i_{ds} - \left(1/C_{dc}\right)V_{dc} i_g \quad (14)$$

where i_g is the external disturbance (total dc current caused by the turbine generator), V_{dc} is DC link voltage, V_{ds} and i_{ds} are d axis voltage and current, V_{qs} and i_{qs} are q axis voltage and current. V_{cd} and V_{cq} are d and q axis converter output voltages. $V_{ds,PI}$ and $V_{qs,PI}$ are the terms regulated by PI controllers, while $V_{ds,coupling}$ and $V_{qs,coupling}$ are decoupling control terms. The grid angle is locked by the synchronous reference frame PLL, which gives a high performance since a balanced grid is in effect. As shown in Fig. 2, k_{inv} is equal to that of PMSG about 16.23, since the same DC bus voltage is in effect, 400 V. V_{dcref} is the DC bus voltage reference value, 400 V. PI gains are selected to meet the desired settling time, 0.0092 s, as;

$$K_{pdg} = k_{sett}L_d \qquad K_{idg} = k_{sett}R_d \quad (15)$$

$$K_{pqg} = k_{sett}L_d \qquad K_{iqg} = k_{sett}R_d \quad (16)$$

where L_d and R_d are inductance and resistance of the line filter. For $k_{sett} = 543$, $K_{pdg} = K_{pqg} = 0.0023$, $K_{idg} = K_{iqg} = 0.25$, the closed loop transfer function of current loops is $TF_{cl} = 543/(s + 543)$, where settling times are 0.0092 s. Electrical time constant of the differential mode choke is also 0.0092 s. The closed loop transfer function of the voltage loop is then given in Eq. (17), for $K_{pdc} = 0.00055$ and $K_{idc} = 0.00005$, as:

$$TF_{cl} = \frac{2.05 \cdot 10^4 s^4 + 1.113 \cdot 10^7 s^3 + 1.012 \cdot 10^6 s^2}{s^6 + 1086s^5 + 3.153 \cdot 10^5 s^4 + 1.113 \cdot 10^7 s^3 + 1.012 \cdot 10^6 s^2} \quad (17)$$

Settling time of Eq. (17) is 0.12 s.

In both control of PMSG and GSC, settling times for inner (current control) loops and outer (voltage and speed control) loops are in good agreement with each other. In this design methodology, right half plane zero of GSC, sampling frequency, switching frequency are design parameters, all of them are considered [19,21]. In Fig. 2, the decoupling based closed loop control scheme is provided for PMSG and GSC.

III. Traditional and Proposed HC Based MPPT Control

In this section, traditional and proposed HC methods are covered.

A. Traditional HC Based MPPT Control

Traditional HC evaluates $\Delta P_g/\Delta\omega$ in finding MPP. So, it is blind to wind speed change, and the problem of wrong directionality arises. This means that lower MPPT efficiency values conclude [22]. Its control law is as:

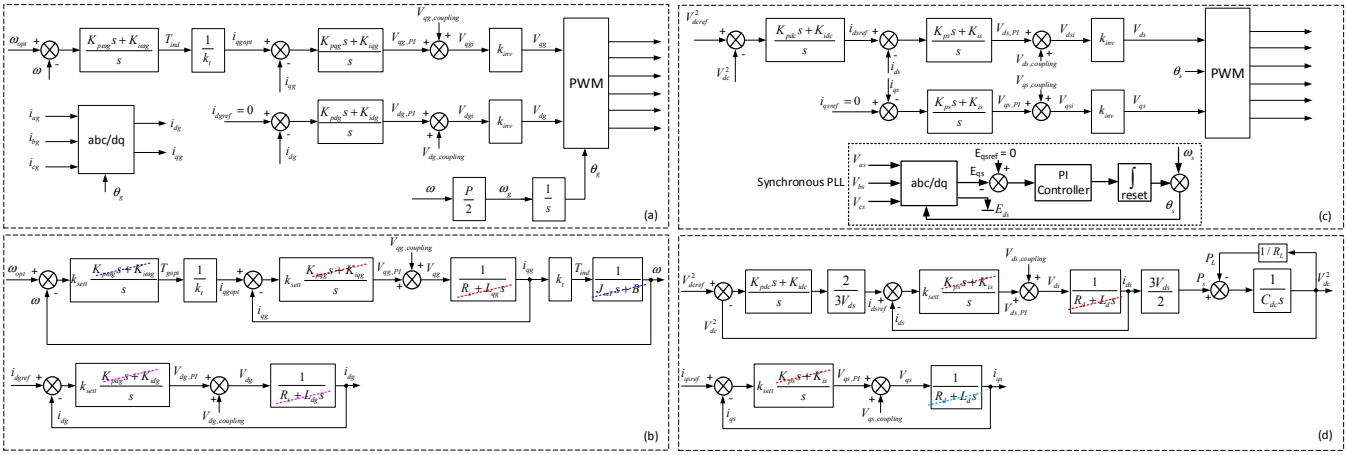

Figure 2. Decoupling based vector control scheme (a), (b) for PMSG (c), (d) for GSC [24]

$$\omega_{opt(k)} = k_m \int_0^{t_{sampling}} sign\left(\Delta P_g \cdot \Delta\omega\right) dt + \omega_{opt(k-1)} \tag{18}$$

If the wind speed increases, T_{in} and P_{in} increases, but traditional HC cannot confirm this increase in P_{in}. That is, in a sampling interval Δt, with increasing wind speed, ω increases by $\Delta\omega$. So, $\Delta P_g \approx 0$ and $\Delta P_{in} \approx \Delta P_j$. That means that the inertia stores about all increment in P_{in}. This implies that it is $\Delta P_g < 0$, which a change in the sign of ΔP_g occurs. Thus, $\Delta P_g < 0$ and $\omega > 0$, and the control law of Eq. (18) starts to decrease ω_{opt} correspondingly. This means that feedback controllers also decrease ω, which is called "wrong directionality". It is very important to note that this drawback occurs because of the wind rotor inertia, which means the traditional HC based MPPT control is not a proper MPPT control method for large wind turbines.

B. Proposed HC Based MPPT Control

Proposed HC based MPPT control law is given in Eq. (19). For an increasing wind speed, either suddenly or slowly, it is always valid that $\Delta P_{in} > 0$ & $\Delta\omega > 0$ and hence the control law can increase ω_{opt} by correctly evaluating $\Delta P_{in}/\Delta\omega$. For a decreasing wind speed, either suddenly or slowly, if $\Delta P_{in} < -\mu_1 P_{inrated}$ & $\Delta\omega < \mu_2\omega_{rated}$, then $\Delta P_g/\Delta\omega$ is calculated instead of $\Delta P_{in}/\Delta\omega$.

So, the control law starts to decrease ω_{opt}. On the other side, if $-\mu_1 P_{inrated} < \Delta P_{in} < 0$ & $-\mu_2\omega_{rated} < \Delta\omega < 0$, namely if the generator speed is driven to an optimum value

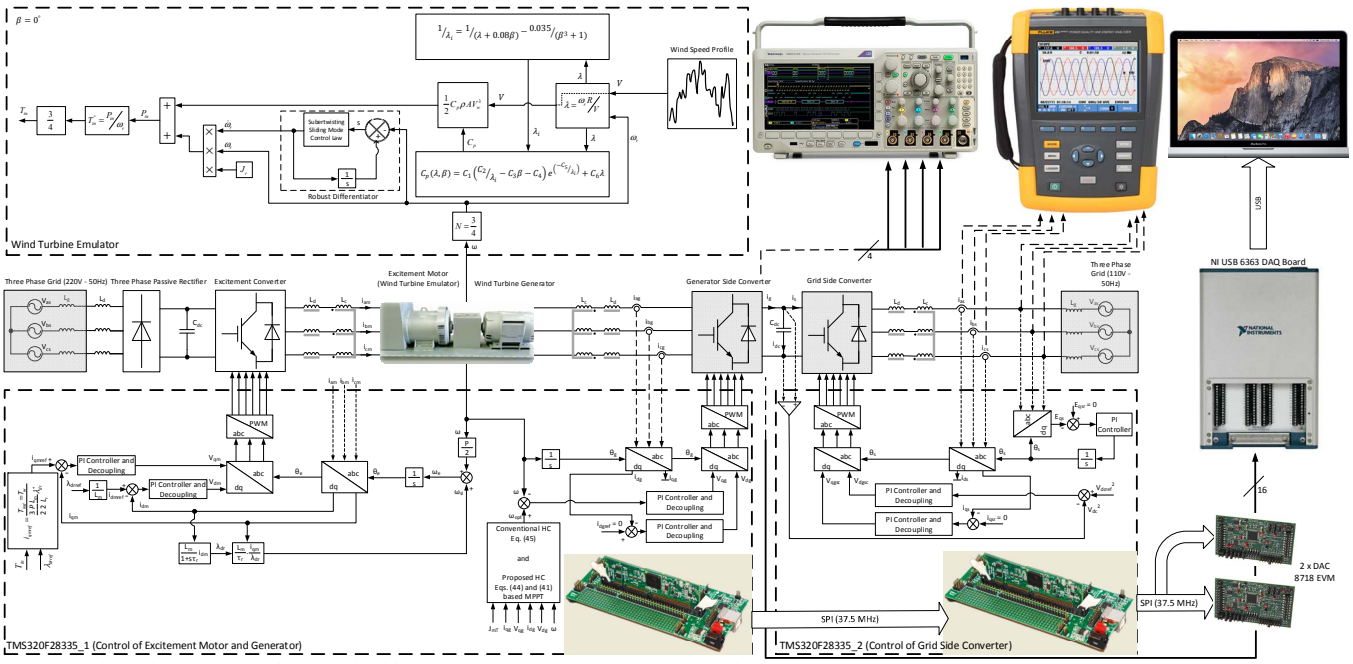

Figure 3. Closed loop control scheme and grid side converter (a), (b) for PMSG (c), (d) for GSC

$$\omega_{opt(k)} = \begin{cases} k_m \int_0^{t_{sampling}} sigmoid\left(\Delta P_{in} \cdot \Delta\omega\right) dt + \omega_{opt(k-1)} : if\left(\Delta P_{in} > 0 \,\&\, \Delta\omega > 0\right) \\ \omega_{opt(k-1)} : if\left(\ 0 > \Delta P_{in} > -\mu_1 P_{inrated} \,\&\, 0 > \Delta\omega > -\mu_2 \omega_{rated}\right) \\ k_m \int_0^{t_{sampling}} sigmoid\left(\Delta P_g \cdot \Delta\omega\right) dt + \omega_{opt(k-1)} : \\ if\left(\Delta P_{in} < -\mu_1 P_{inrated} \,\&\, \Delta\omega < -\mu_2 \omega_{rated}\right) \end{cases} \quad (19)$$

that the turbine operates at MPP, the control law keeps $\omega_{opt(k)} = \omega_{opt(k-1)}$. Consequently, the proposed HC drives the turbine speed to MPP without being affected by the turbine

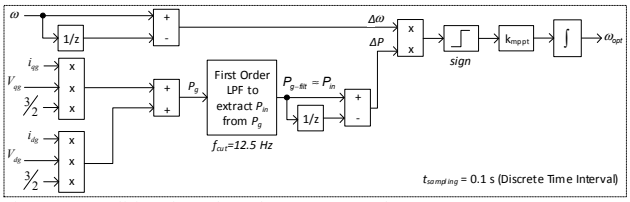

Figure 4. Traditional HC based MPPT control

inertia. In Figs. 4 and 5, traditional and proposed HC based MPPT control schematic diagrams are provided respectively.

This study differs from the previous ones [23,24]. from those aspects as: 1. As perturbation function, sigmoid function instead of commonly used signum function "$sigmoid = 2 \cdot \left(-0.5 + \frac{1}{1+e^{-5u}}\right)$" is used in the proposed HC control law to mitigate the chattering effect in ω_{opt}. The robust differentiator is used for differentiating the generator speed with respect to time in the wind turbine emulator and in the proposed MPPT. In Figs. 4 and 5, traditional and proposed HC are given together.

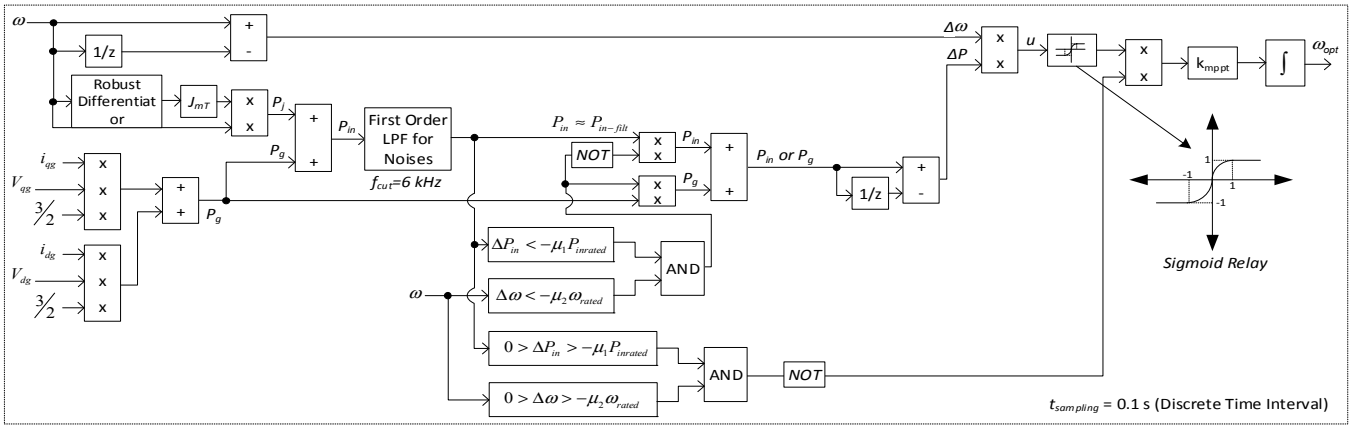

Figure 5. Proposed HC based MPPT control

C. Robust Differentitator

Robust differentiator is generally used to smoothly differentiate noisy signals with respect to time. In power electronics, nearly all signals are of high noise, robust differentiator is commonly employed for this purpose [25]. Its control law is as follows:

$$\begin{aligned} u &= \dot{\omega}_r = -\alpha \left|s\right|^{1/2} sign(s) + v \\ \dot{v} &= -0.5\beta sign(s) \end{aligned} \quad (20)$$

In the experimental verification stage of this study, it is chosen as $\alpha = 201.4, \beta = 52.3$. Robust differentiator has a global asymptotic stability, for the stability analysis of robust differentiator, one can refer to [25] for details.

IV. Experimental Results

A picture of the experimental set-up is provided in Fig. 7. As seen from the figure, there are two converters. One is three phase inverter account for driving IM to emulate wind turbine. The other is back to back converter consisting of GSC and a three-phase inverter responsible for driving PMSG. All inverters are two-level inverters.

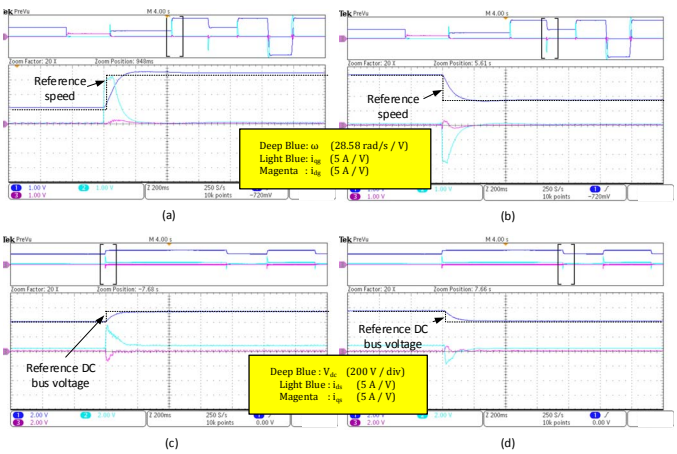

Figure 6. Step responses for the control of (a,b) PMSG (c,d) GSC

As a control unit, TMS320f28335 DSP is used, current and voltage transducers are LA 55p and LV 25p respectively. All the parameters of the set-up are given in Table I.

TABLE I. ALL PARAMETERS OF THE CONTROL SYSTEM AND EXPERIMENTAL SET-UP

Parameter	Notation	Value
Rated turbine input power	$P_{inrated}$	2.5 kW
Air density, Turbine radius	ρ, R	1.14 kg/m^3, 1.3 m
C_p coefficients	C_1, C_2, C_3, C_4, C_5, C_6	0.5176, 116, 0.4, 5, 21, 0.0068
Rated wind speed	V_{rated}	12 m/s
Optimal power coefficient	C_{pmax}	0.48

Wind rotor inertia	J_r	6 kg/m^2
Gear ratio	-	3/4
Rated wind rotor speed	ω_{rrated}	75 rad/s
Line filter for grid side converter	R_d, L_d	0.25 Ω, 2.3 mH
Common mode filter	L_c	15 mH
DC bus capacitor	C_{dc}	3400uF
Grid phase voltages	V_{as}, V_{bs}, V_{cs}	110 Vrms, 50 Hz
DC bus voltage	V_{dc}	400V
IGBT driver	*SEMIKRON*	Skyper 32 PRO R
IGBT module	*SEMIKRON*	SKM150GB12T4
Current and voltage sensors	*LEM*	LA55-P and LV25-P
Diode module	*SEMIKRON*	SKKD100/12
Heatsink	*SEMIKRON*	0.12K/W
Stator phase resistance	R_s	0.25 Ω
Stator phase inductance	L_s	L_{qg}=3.2 mH, L_{dg}=1.7 mH
Rotor magnetizing flux	λ_m	0.21 Wb
Rated values	*PMSG*	5 kW, 4 poles, 400 V, 15 A, 2000 rpm, 24 Nm
Generator inertia	J_g	0.00657 kgm^2
Torque constant	k_t	1.26 Nm/A
Parameters for proposed and traditional HC	k_{mppt}=4,0, μ_1=0.0036, μ_2=0.0001	

IGBTs are SKM150GB12T4 and IGBT drivers are Skyper 32 Pro R. First experimental results are presented in Fig. 6 to verify tuning of PI controllers designed for the control of PMSG and GSC. As seen from Fig. 5, settling times take approximately 0.15 s and 0.12 s for the control of PMSG and GSC respectively. Tuning aims of PI controllers in section III are very closely confirmed by experimental results.

In Fig. 7, traditional and proposed HC based MPPT control methods are compared to each other in terms of the captured power from the wind for the same profile. P_{OPT_TSR} is the maximum power available in the wind, calculated by TSR based MPPT approach. As seen from Fig. 7, traditional HC based MPPT control fails to track MPP in both transients and steady state. Wind speed variation with both positive and negative slope cause the wrong directionality in transients. At the same time, it can be observed a low performance in steady state, as well. The algorithm cannot keep generator speed at optimum value stably. However, proposed HC based MPPT control works with relatively higher performance in both transient and steady state. First, there is no wrong directionality and the algorithm can track MPP against increasing and decreasing wind speed.

It is important to note that total inertia of PMSG and IM 0.0326 kgm^2. This inertia value can be neglected, and traditional HC based MPPT control can ensure a high energy efficiency. However, the turbine emulator can emulate extra inertia, too. In this study, as a propeller inertia, an extra 6 kgm^2 is emulated, which this value cannot be neglected. As demonstrated in Fig 8 (b), traditional HC based MPPT control omits the turbine inertia and hence wrong directionality happens in the turbine response, under especially sudden variation of wind speed. However, proposed HC based MPPT control consider the turbine inertia, and it can keep P_{in} at about P_{OPT_TSR} in transient and steady state. Traditional HC based MPPT control can capture 241.62 kWs from the wind profile

(a) (b)

Figure 7. Experimental setup (a) the complete hardware (b) only power converters.

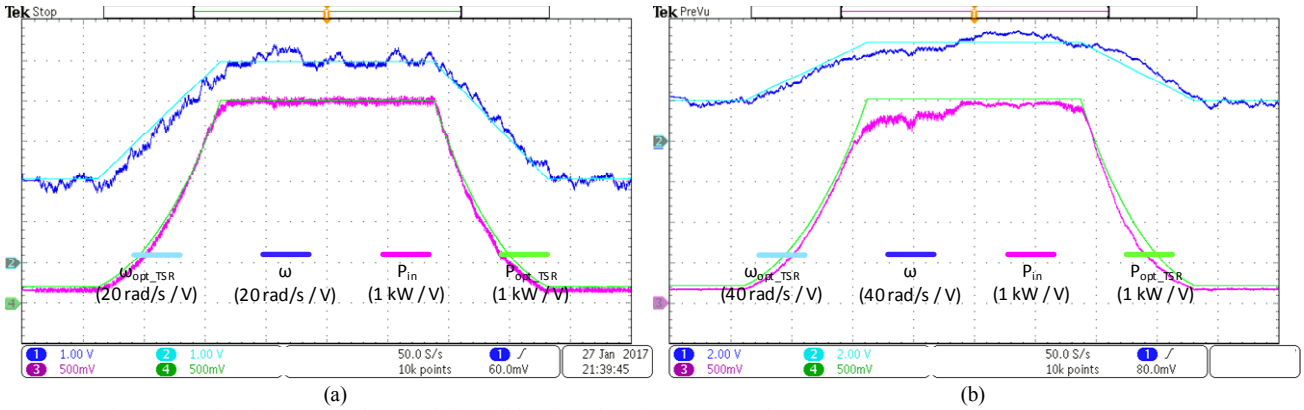

(a) (b)

Figure 8. Experimental results of (a) proposed HC and (b) traditional HC based MPPT control

given in Fig. 7. On the other side, 261.48 kWs are harvested by the proposed HC based MPPT control from the same wind profile. Consequently, the proposed MPPT control yields an increase in MPPT efficiency by 8.22 %.

V. CONCLUSIONS

This study proposes a new MPPT control method for especially large wind turbines. For large wind turbines, it is a well-known fact that the generator output power is greatly influenced by the turbine rotor inertia. For example, while the turbine rotor speeds up, the inertia nearly stores all the power available in the wind. On the other hand, while the rotor slows down, the inertia releases nearly all the power stored. In these circumstances, it is not possible to implement a correct MPPT control for large wind turbines without considering the inertia related dynamics. The proposed MPPT control method here takes the turbine rotor inertia along with its related dynamics into consideration, and hence it can track the MPP correctly. Experimental results obtained with a wind turbine emulator shows that it is likely to increase MPPT efficiency up to 10,0 %.

ACKNOWLEDGMENT

This study is supported by the Scientific and Technological Research Council of Turkey (TUBITAK) Research Fund (Project No. 114E159), the authors thank to the TUBITAK.

REFERENCES

[1] V. Yaramasu, and B. Wu, "Model Predictive Control of Wind Energy Conversion Systems," Wiley–IEEE Press, IEEE Press Series on Power Engineering, February 2017, pp-42-44.

[2] H. Fathabadi, "Novel high-efficient unified maximum power point tracking controller for hybrid fuel cell/wind systems," Applied Energy, vol.183, pp. 1498-1510, 2016.

[3] K.H. Kim, T.L. Van, D.C. Lee, S.H. Song, and E.H. Kim, "Maximum output power tracking control in variable-speed wind turbine systems considering rotor inertial power". IEEE transactions on industrial electronics, vol. 60, no. 8, pp. 3207-3217, 2013.

[4] C. Huang, F. Li, and Z. Jin, "Maximum power point tracking strategy for large-scale wind generation systems considering wind turbine dynamics", IEEE transactions on industrial electronics, vol. 62, no. 4, pp. 2530–2539, 2015.

[5] C. Tang, W.L. Soong, P. Freere, M. Pathmanathan and N. Ertugrul, "Dynamic wind turbine output power reduction under varying wind speed conditions due to inertia", Wind Energy, vol. 16, no. 4, pp. 561-573, 2013.

[6] A.S. Satpathy, N. Kastha, D. Kishore, and N. Sahoo, "Control scheme for a stand-alone wind energy conversion system." IEEE Transactions on Energy conversion, vol. 29, no. 2, pp. 418–425, 2014.

[7] S. Ghasemi, A. Tabesh and J. Askari-Marnani "Application of fractional calculus theory to robust controller design for wind turbine generators." IEEE Transactions on Energy conversion, vol. 29, no. 3, pp. 780–787, 2014,

[8] Z. Chen, M. Yin, Y. Zou, K. Meng and Z. Dong, "Maximum Wind Energy Extraction for Variable Speed Wind Turbines with Slow Dynamic Behavior," IEEE Transactions on Power Systems, vol. 32, no. 4, pp. 3321-3322, July 2017.

[9] Q. Wang and L. Chang, "An intelligent maximum power extraction algorithm for inverter-based variable speed wind turbine systems," IEEE Transactions on Power Electronics, vol. 19, no. 5, pp. 1242-1249, Sept. 2004.

[10] R. Aubrée, F. Auger, M. Macé, and L. Loron, "Design of an efficient small wind-energy conversion system with an adaptive sensorless MPPT strategy", Renewable Energy, vol. 86, pp. 280-291, Feb. 2016.

[11] C. Tang, M. Pathmanathan, W. L. Soong, and N. Ertugrul, "Effects of inertia on dynamic performance of wind turbines," Australasian Universities Power Engineering Conference, IEEE, 2008, pp. 1-6.

[12] E. Koutroulis and K. Kalaitzakis, "Design of a maximum power tracking system for wind-energy-conversion applications," IEEE transactions on industrial electronics, vol. 53, no. 2, pp. 486-494, Apr. 2006.

[13] S. M. R. Kazmi, H. Goto, H. J. Guo and O. Ichinokura, "A Novel Algorithm for Fast and Efficient Speed-Sensorless Maximum Power Point Tracking in Wind Energy Conversion Systems," IEEE Transactions on Industrial Electronics, vol. 58, no. 1, pp. 29-36, Jan. 2011.

[14] H. Fathabadi, "Novel Maximum Electrical and Mechanical Power Tracking Controllers for Wind Energy Conversion Systems," IEEE Journal of Emerging and Selected Topics in Power Electronics, vol. 5, no. 4, pp. 1739-1745, Dec. 2017.

[15] W. Li, M. Yin, Z. Chen, and Y. Zou, "Inertia compensation scheme for wind turbine simulator based on deviation mitigation," Journal of Modern Power Systems and Clean Energy, vol. 5, no: 2, pp. 228-238, 2017.

[16] M. Karabacak, H. I. Eskikurt, "Speed and current regulation of a permanent magnet synchronous motor via nonlinear and adaptive backstepping control", Mathematical and Computer Modelling, vol. 53, no. 9-10, pp. 2015-2030, 2011,

[17] M. Karabacak, H. I. Eskikurt, "Design, modelling and simulation of a new nonlinear and full adaptive backstepping speed tracking controller for uncertain PMSM," Applied Mathematical Modelling, vol. 36, no. 11, pp. 5199-5213, 2012.

[18] J. Dannehl, C. Wessels and F. W. Fuchs, "Limitations of Voltage-Oriented PI Current Control of Grid-Connected PWM Rectifiers with LCL Filters," in IEEE Transactions on Industrial Electronics, vol. 56, no. 2, pp. 380-388, Feb. 2009.

[19] M. Karabacak, "A Novel Nonlinear and Adaptive Control of Grid Connected Inverters", Journal of Circuits, Systems and Computers, vol. 25, no. 11, pp. 1-25, 2016.

[20] T. S. Lee, "Input-output linearization and zero-dynamics control of three-phase AC/DC voltage-source converters," IEEE transactions on industrial electronics. vol. 18 pp. 11-22, 2003.

[21] Kiyong Kim and R. C. Schaefer, "Tuning a PID controller for a digital excitation control system," in IEEE Transactions on Industry Applications, vol. 41, no. 2, pp. 485-492, March-April 2005.

[22] Z. M. Dalala, Z. U. Zahid, W. Yu, Y. Cho and J. S. Lai, "Design and Analysis of an MPPT Technique for Small-Scale Wind Energy Conversion Systems," in IEEE Transactions on Energy Conversion, vol. 28, no. 3, pp. 756-767, Sept. 2013.

[23] M. Karabacak, L. M. Fernández-Ramírez, T. Kamal and S. Kamal, "A New Hill Climbing Maximum Power Tracking Control for Wind Turbines With Inertial Effect Compensation," in IEEE Transactions on Industrial Electronics, vol. 66, no. 11, pp. 8545-8556, Nov. 2019.

[24] M Karabacak, "A new perturb and observe based higher order sliding mode MPPT control of wind turbines eliminating the rotor inertial effect," Renewable Energy, vol. 133, pp. 807-827, 2019.

[25] A. Levant, Robust exact differentiation via sliding mode technique, Automatica, vol.34, no. 3, pp. 379-384, 1998.